


Adamantane/Cucurbituril: A Potential Pretargeted Imaging Strategy in Immuno-PET

Molecular Imaging
Volume 17: 1-7
© The Author(s) 2018
Article reuse guidelines:
sagepub.com/journals-permissions
DOI: 10.1177/1536012118799838
journals.sagepub.com/home/mix


Martin G. Strebl, PhD¹, Jane Yang, BS¹, Lyle Isaacs, PhD², and Jacob M. Hooker, PhD¹

Abstract

Positron emission tomography (PET) imaging with biological macromolecules greatly expands the possibilities of molecular imaging. There are, however, practical aspects limiting the potential of the approach, including the dosimetric consequences of the slow kinetics of radiolabeled biomacromolecules. Pretargeting strategies have led to impactful improvements in the field but are themselves limited by shortcomings of available bioconjugation methodology. We report our initial findings concerning the suitability of the adamantane/cucurbit[7]uril system for pretargeted immuno-PET imaging and provide proof-of-concept PET/computed tomography imaging experiments to establish the stability and rapid formation of host–guest complexes in vivo. The adamantane/cucurbit[7]uril system itself without antibody conjugation has shown remarkably fast association kinetics and clearance in vivo. We further demonstrate the modulation of biodistribution achievable by cucurbituril complexation with relevance for pharmaceutical formulation as well as the radiosynthetic access to relevant reporter molecules labeled with ¹¹C or ¹⁸F. This work, an early proof-of-concept, supports the notion that the adamantane/cucurbit[7]uril system warrants further exploration in pretargeted PET imaging applications.

Keywords

PET, cucurbituril, bioconjugation, antibody, imaging

Introduction

The use of biological imaging agents in positron emission tomography (PET) and other molecular imaging techniques has been a long-standing endeavor.¹⁻³ New technologies hold great promise toward early detection and improved treatment strategies of cancer and other diseases.^{4,5} Antibody-based imaging has certain limitations that have slowed its introduction to routine clinical practice⁶ but shows high potential. A primary caveat when considering the use of antibody-based imaging is the slow distribution and clearance kinetics of antibodies,⁷ which can greatly lengthen the time between injection and scanning, promoting the use of long-lived isotopes with poor dosimetry profiles.^{7,8} ⁸⁹Zr-based immuno-PET, for example, has a mean effective dose significantly higher than that of ¹¹¹In- and ^{99m}Tc-based tracers which can limit the repeatability of the application.⁹

Systems to partially overcome specific limitations have been reported,^{8,10-14} with a general solution still outstanding. In order to circumvent the problems arising from the large size of antibodies, curtailed variants like affibodies have been developed,¹⁵ with a trade-off between binding affinity and size.

A more fundamentally different approach are the so-called “pretargeting” strategies,¹⁶ which make the antibody a surrogate target for a second, isotope-bearing reporter with more favorable biodistribution properties. That way, the slow antibody kinetics are decoupled from the actual imaging, and the use of shorter lived isotopes is possible.¹⁷ Bispecific antibodies with affinity for a disease-related antigen as well as a radioactive reporter molecule were the first actualization of that strategy, with limited success.⁶ The widespread use of bispecific antibodies is ultimately hampered by the difficulty in

¹ Athinoula A. Martinos Center for Biomedical Imaging, Massachusetts General Hospital and Harvard Medical School, Charlestown, MA, USA

² Department of Chemistry and Biochemistry, University of Maryland, College Park, MD, USA

Submitted: 22/05/2018. Revised: 20/07/2018. Accepted: 04/08/2018.

Corresponding Author:

Jacob M. Hooker, Athinoula A. Martinos Center for Biomedical Imaging, Massachusetts General Hospital, Boston, MA, USA.

Email: hooker@nmr.mgh.harvard.edu



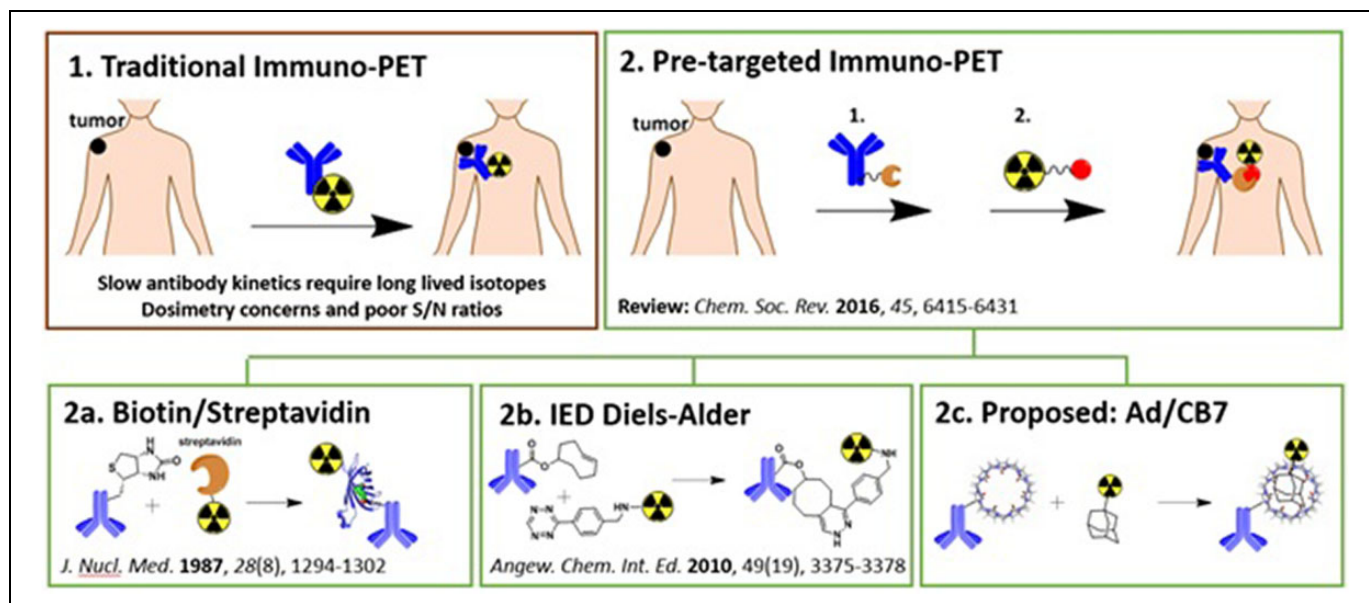


Figure 1. Strategies in immuno-PET imaging. 1, Classic immuno-PET imaging employs antibodies bearing long-lived radioisotopes that match slow antibody kinetics, limiting its application due to poor dosimetry.^{4,23} 2, Pretargeting temporally and spatially decouples the antibody distribution and the radiovisualization steps.¹⁶ Different strategies can be employed, for example 2a. Biotinylated antibodies that are visualized after initial clearance with radiolabeled streptavidin¹⁵ or 2b. Trans-cyclooctene-tagged antibodies that are visualized with radiolabeled tetrazine derivatives via inverse electron demand diels alder reactions.³² 2c, We propose that cucurbituril-tagged antibodies can be visualized with radiolabeled adamantane derivatives, which could circumvent limitations inherent to other bioconjugation strategies. PET indicates positron emission tomography.

designing and producing such agents.^{18,19} A more straightforward solution exploiting the high binding affinity between biotin and streptavidin²⁰ has been demonstrated, but limitations include the presence of endogenous biotin and the immunogenicity of streptavidin-derived agents.²¹⁻²³ Another variation is based on complementary DNA strands, but such systems suffer from rapid degradation *in vivo*.²⁴ While a number of other pretargeted strategies for PET imaging have shown immense promise, they have been restricted at least in part by the lack of appropriate *in vivo* bioconjugation methodology.²³ An inverse electron demand (IED) Diels-Alder strategy, for example, shows great promise, but limitations include the association kinetics that are much lower than that of noncovalent high-affinity interactions used in humans and that trans-cyclooctene can be deactivated via copper-containing proteins.^{23,25} Herein, we report proof-of-concept experiments suggesting that a cucurbituril/adamantane-based system could ameliorate shortcomings of current bioconjugation methodologies in pretargeted immuno-PET (Figure 1).

Cucurbiturils are macrocyclic glycoluril oligomers that are broadly used in supramolecular chemistry as hosts for small hydrophobic organic residues.^{26,27} Interest has been demonstrated for their use as additives in pharmaceutical formulations similar to cyclodextrin.²⁸ Toxicity and cytotoxicity of cucurbiturils has been demonstrated to be low,²⁹ but immunogenicity has yet to be investigated. Adamantane derivatives have a particularly high affinity to cucurbit[7]uril (CB7),³⁰ and association kinetics are fast³¹ The advantage of this system is that the extremely strong and fast association of CB7 with a wide range

of adamantyl-bearing molecules allows for flexibility around the reporter design and can be tailored toward a number of specific applications, including pretargeted immuno-PET. For reference, adamantane guests in CB7 have equilibrium constants in the range of 10^{10-15} (M^{-1}).³⁰

Results and Discussion

In immuno-PET, some hurdles arise from the slow distribution kinetics of antibodies. Pretargeting surface antigens with a CB7-bearing antibody and subsequent imaging with a radiolabeled adamantane-containing small molecule (reporter) with tunable pharmacokinetics could allow the use of short-lived isotopes to image targets through pretargeted immuno-PET. Azide-linked CB7 for antibody labeling can be readily synthesized³³ for future studies with a CB7-antibody complex. An advantage over available systems lies in the flexibility around the design of the reporter, with adamantane being a relatively small, unreactive entity. Due to its lipophilicity and ability to ensure drug stability, the adamantyl scaffold has enhanced pharmacokinetics of the modified drug candidates.³⁴ Selecting a cell-permeable compound as a reporter, for example, should enable imaging of internalized antibodies, making the concept much more generally applicable.

We were interested to investigate the suitability of the adamantane-CB7 interaction for pretargeting purposes. In order to do so, 2 basic properties had to be investigated: (1) stability of a preformed adamantane-CB7 complex *in vivo* and (2) fast enough association kinetics to ensure effective *de novo* complex formation *in vivo*.

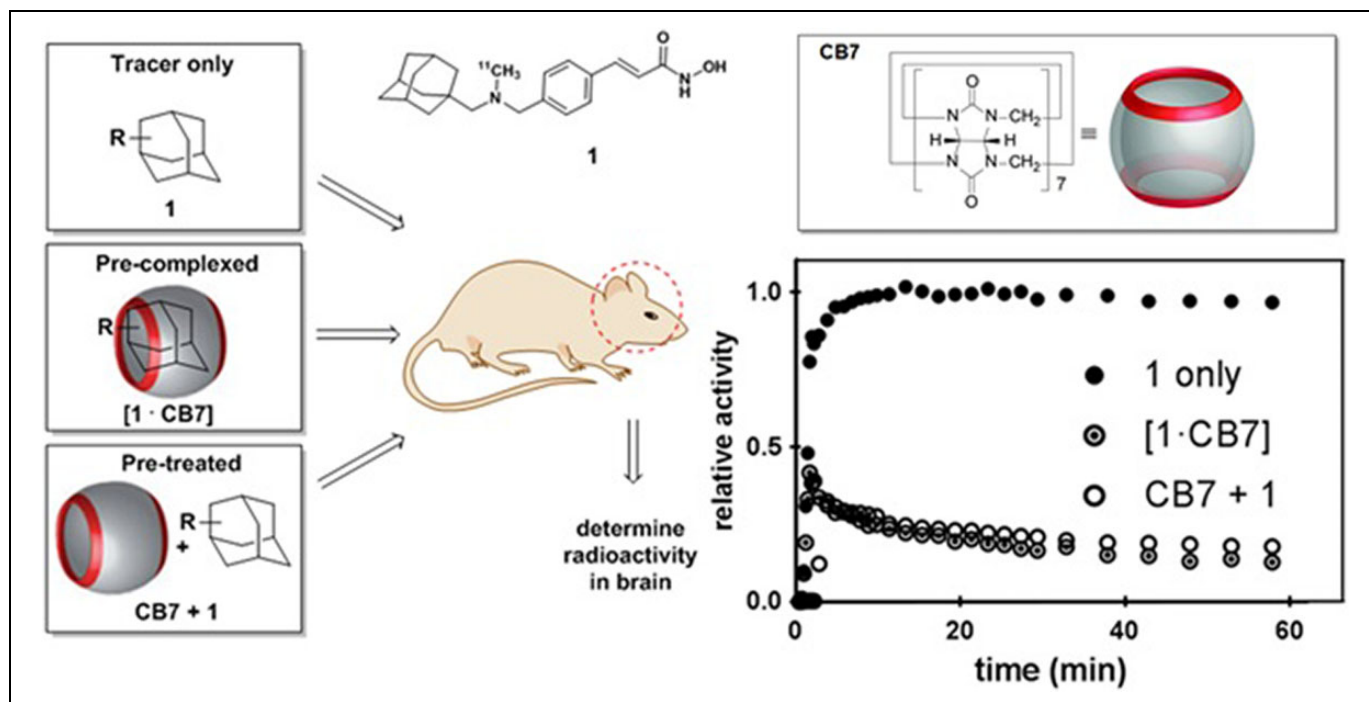


Figure 2. Changes in brain penetration of martinostat (**1**) in the presence of CB7. **1** Exhibits high brain uptake. When complexed by CB7 prior to administration (“precomplexed”), practically no radioactivity is observed in the brain. The effect can be reproduced by “pretreating” the animal with systemic CB7 prior to radiotracer administration. CB7 indicates cucurbit[7]uril.

We decided to use an existing radiotracer with a substituted adamantane moiety— ^{11}C Martinostat (**1**)—to investigate these fundamental aspects of the proposed system. In Figure 2, the results of PET imaging experiments to address these concerns are displayed. The tracer exhibits high brain penetration in rodents, while CB7 should show very limited blood–brain barrier penetration based on its size and polarity. When the radiotracer **1** was treated with CB7 before administration, approximately 90% less radioactivity was taken up in the brain. We preliminarily conclude that these results show the potential of complexes of adamantane-containing small molecules with CB7 is stable *in vivo* on a PET imaging timescale for a pretargeting strategy. When animals were treated intravenously with CB7 before administration of **1** (“pretreated”), the same result was obtained: After an initial spike, practically no radioactivity was retained in the rodent brain. We therefore conclude that condition **2** is fulfilled, the kinetics of the CB7–adamantane system, without antibody conjugation, is fast enough for complex formation *in vivo*. However, we should note that although compound **1** freely diffuses cell membranes and accesses privileged cell compartments like the nucleus, it remains unclear the extent to which internalized/vesicularized moieties (eg, antibodies) could be engaged with adamantane/CB7 systems.

We were further able to demonstrate in mouse whole-body PET scans that the concept is more general, by comparing the distribution behavior of 3 radiolabeled molecules by themselves in comparison to the host–guest complex with CB7. These data suggest that CB7 dominates the biodistribution of

guest molecules, which discloses the distribution behavior of CB7 *in vivo*, which is highly relevant with respect to pharmaceutical applications of the host.

As seen in the left row of images in Figure 3, 3 different C-11-labeled molecules **2** to **4** showed distinct distribution patterns when administered individually, but the images look practically identical (right row) for all 3 tracers when precomplexed with CB7. The uncomplexed molecules clearly show different amounts of renal versus hepatic clearance and possibly different metabolic cleavage of methanol, which could be responsible for the excellent clearance of **2**. For a suitable reporter, clearance behavior can be optimized to detect lesions in particular areas of interest with higher specificity, that is, a compound with exclusively renal clearance would be desirable to detect regions of interest around the liver. When complexed with CB7, the intrinsic properties of the probes are masked and they all behave essentially the same. It is interesting to note that in all 3 cases, the same change in distribution over time was observed, which is visualized for one animal in the Supporting video. After injection in the lateral tail vein, the tracers pass the heart and after a brief period of systemic distribution are filtered out by the kidneys and passed on to the bladder. In averaged images of later time points (30–60 minutes post-time of injection [TOI]), as shown on the right side of Figure 3, the kidneys are the most prominent radioactive feature beneath the bladder. It is important to note that while brain uptake may not be a primary measure of this system’s effectiveness, it is indicative of the potential of the system’s success in future pretargeting experiments with antibody conjugation.

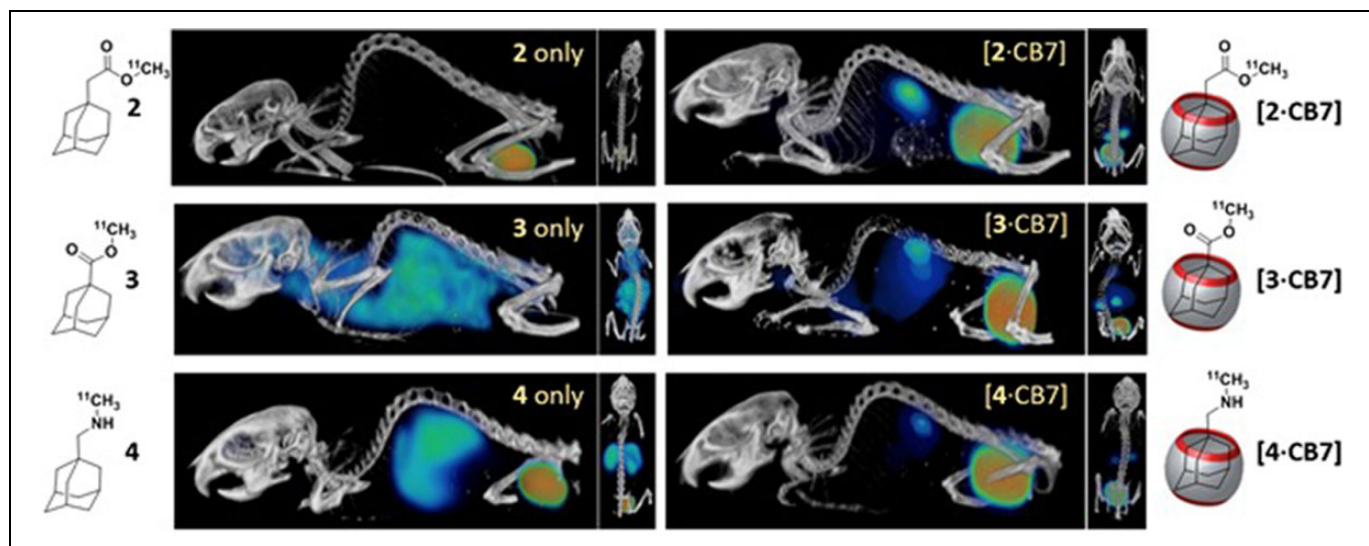


Figure 3. Biodistribution of **2** to **4** in the absence and presence of CB7. Three different ^{11}C -labeled molecules show distinct biodistribution in mice when administered individually. The left image column represents sagittal views of a 3-dimensional rendering of dynamic PET data averaged from 30 to 60 minutes post-radiotracer injection overlaid on a CT of the same animal. 1 mg/mL of CB7 was used for precomplexed experiments. The transverse view to the right shows the same animal from a different perspective for clarity. In the right column of images, the distribution of the same ^{11}C -labeled molecules is shown when precomplexed with CB7. CB7 indicates cucurbit[7]uril; PET, positron emission tomography; CT, computed tomography.

The experiments were carried out with low *effective* specific activity reporters. It is conceivable that the mass of injected reporter is a variable that needs to be optimized for distinct imaging protocols, and the molecules employed can all be synthesized in high specific activity simply by adding additional purification steps.

The short half-life of ^{11}C presents an intrinsic practical limitation to the proposed application. ^{18}F is easily available throughout the continental United States, as it is the most commonly used positron emitter in the clinical setting, and fluorinated tracers are currently the most useful in a logistic capacity and allow for more stable syntheses due to the longer half-life compared to ^{11}C . More recent advances in ^{18}F fluorination chemistry allow the direct labeling of adamantyl residues with ^{18}F .³⁵ In order to probe whether associated structural changes disrupt the complexation, experiments analogous to Figure 3 were conducted with ^{18}F -labeled fluoroadamantylamine in Sprague-Dawley rats. As seen in Figure 4B and C, not only was the retention time of the probe on a high-performance liquid chromatography (HPLC) shifted significantly when CB7 was added but also the ratio of kidney-to-liver uptake at later time points was increased over 4-fold consistent with the biodistribution changes observed earlier. The change in distribution was reproducible by injecting CB7 separately 5 minutes before injection of radiotracer. This alludes to the potential that association kinetics will be sufficient for future experiments of this system with antibody-conjugated CB7. It is further worth noting that no bone uptake of fluoride was observed, indicating metabolic stability of the C–F bond on a PET timescale, which is atypical for aliphatic fluorides. These results suggest that fluoroadamantyl moieties should receive more attention in the

design of ^{18}F -radiotracers generally, since they are practically accessible and stable, yet to our knowledge not utilized. While formal H to F substitutions may lead to purification issues, alternative aliphatic fluorination methods are available that employ starting materials more easily separable from fluorides than the unsubstituted compounds (eg, carboxylates).³⁶

Summary

We establish herein the preliminary compatibility of the adamantane/CB7 host–guest complex interaction with the concept of pre-targeted immuno-PET. We show for a variety of radiolabeled reporters that association complexes with CB7, albeit without antibody conjugation, are stable and form rapidly *in vitro* and *in vivo* and that biodistribution of radiolabeled adamantane derivatives can be fundamentally changed by addition of CB7 for both molecules labeled with ^{11}C and ^{18}F . In addition to our preliminary findings, we report a potential caveat in that the extremely rapid complex will leave complex formation in the blood which could be a major hurdle. We also note the possibility of the rate of clearance of the molecules to be too rapid for tumor targeting. We are hopeful that this concept will be widely applicable to pre-targeted immuno-PET as well as pre-targeted radiotherapy. Applications of CB7 in pharmaceutical formulation can profit from information about its *in vivo* distribution disclosed herein as well.

Materials and Methods

Radiosynthesis

Compound 1 (Martinostat) was prepared as previously described.³⁷ Molecular weight: 354.49 g/mol.

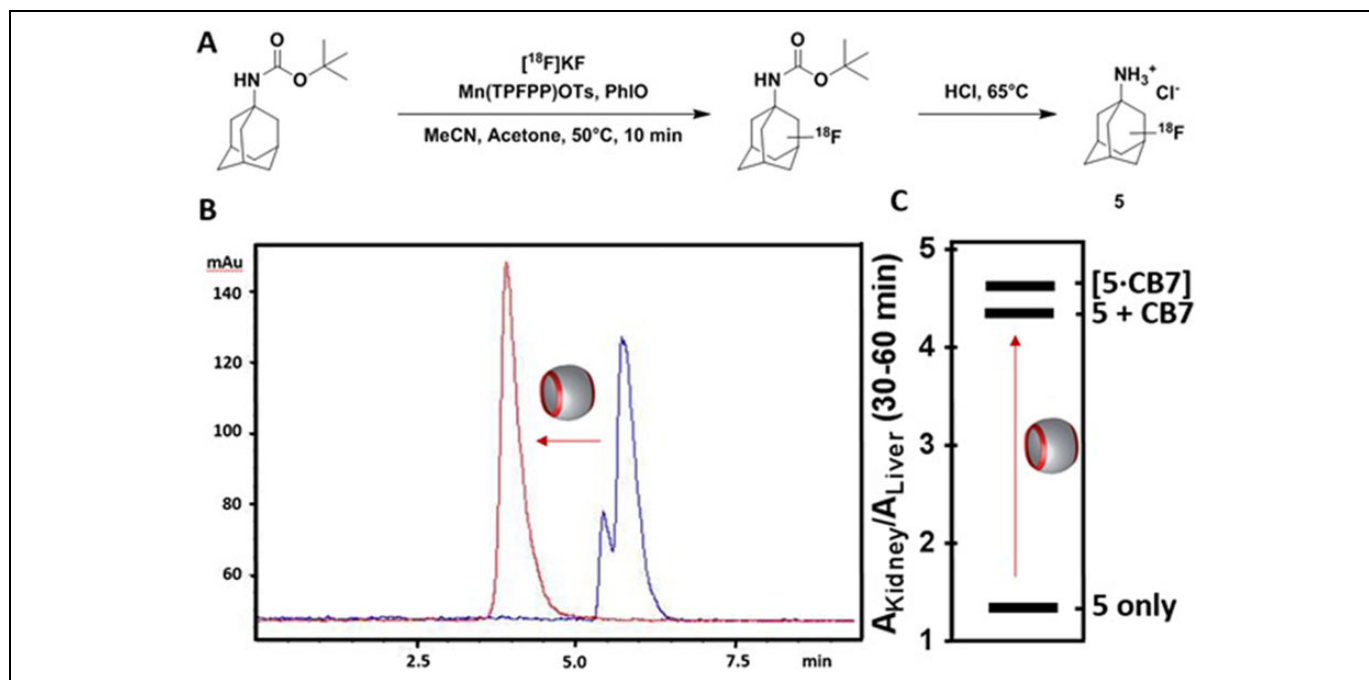


Figure 4. Fluorinated adamantane is a suitable reporter moiety. (A) Scheme of the radiosynthesis of fluoroadamantylamine **5** used for imaging; (B) change in HPLC retention behavior upon addition of CB7 to the tracer; (C) ratio of average radioactivity retained in rat kidneys over liver (averaged 30-60 minutes), which increases 4-fold when **5** is complexed by CB7 or when the animal is pretreated with CB7. HPLC indicates high-performance liquid chromatography; CB7, cucurbit[7]uril.

Compounds 2-4: [^{11}C]MeI was trapped in 0.6 mL dimethyl sulfoxide (DMSO). The solution was partitioned into 3 vials each containing 2 mg K_2CO_3 and 2 mg of either 1-adamantanecarboxylic acid, 1-adamantane carboxylic acid, or 1-adamantanemethylamine. The vials were capped and heated at 85°C for 5 minutes, then each diluted to 20 mL and passed through an Oasis C-18 SPE cartridge. The cartridge was washed with water and the product eluted with 1 mL ethanol. Activity yields obtained 47% (adamantanecarboxylic acid methyl ester (**2**)), 27% (adamantanecarboxylic acid methyl ester (**3**)), and 35% (N-methyl-1-adamantanemethylamine (**4**)).

Compound 5: [^{18}F]fluoride was passed through and trapped on a Chromafix PS-HCO $_3$ IEX cartridge which had been conditioned with 1 mL of 1 mg/mL K_2CO_3 solution and equilibrated with 5 mL of deionized water. The cartridge was washed with 5 mL of deionized water, and residual water was removed with air purge. Then a solution containing 16 mg of Mn(TPFPP)OTs and 0.5 mL acetone was used to slowly elute the [^{18}F] fluoride into a dram vial containing 62.8 mg of 1-(Boc-amino)-adamantane, 80 mg of PhIO, 0.4 mL of dry acetonitrile, and a stir bar. The resulting solution was capped and stirred at 50°C for 10 minutes. After 10 minutes, 1 mL of dry acetonitrile was added, and the resulting solution was pushed through a Phenomenex PTFE membrane $0.45\ \mu\text{m} \times 15\ \text{mm}$ syringe filter for semi-preparatory HPLC analysis. Using an Agilent Eclipse XDB-C18 ($9.4\ \mu\text{m} \times 250\ \text{mm} \times 5\ \mu\text{m}$) column and a water/acetonitrile (95:5 to 5:95 over 25 minutes at 4 mL/min) gradient with 0.1% trifluoroacetic acid mobile phase, the desired fraction was collected around 15 minutes. The fraction

was loaded onto a Phenomenex Strata X 33u 500 mg/6 mL cartridge which had been conditioned with ethanol and water. The cartridge was washed with 10 mL of sterile water for injection, and residual water was removed with air purge. The product was eluted with 3 mL of ethanol, the first and third milliliter of eluate was discarded. HCl (conc) of 80 μL was added to the vial and heated at 65°C for 30 minutes. sodium carbonate buffer (pH 9.4) of 1 mol/L was added to neutralize the solution; 0.9% saline was added to make a 10 mL isotonic solution. The resulting solution was pushed through a Millex-GP sterilizing filter. The final product solution was analyzed under HPLC using an Agilent XDB-C18 ($4.6\ \mu\text{m} \times 150\ \text{mm} \times 5\ \mu\text{m}$) column and a water/acetonitrile gradient (95:5 to 5:95 over 18 minutes at 1 mL/min) with 0.1% trifluoroacetic acid.

To prepare CB7 complexes, 1 mL of formulated dose was combined with 1 mg of CB7 dissolved in 10 μL of DMSO.

Imaging

Animal preparation. All treatment and imaging experiments were performed in accordance with procedures approved by the Institutional Animal Care and Use Committee at the Massachusetts General Hospital.

Rats. Three male Sprague-Dawley rats (Charles River Laboratories) were used for PET imaging. Anesthesia was achieved with isoflurane in medical oxygen carrier (3% for induction, 2% for maintenance). For intravenous administration, a catheter with an extension line was placed in a lateral tail

vein. One animal received a second catheter in the opposing lateral tail vein for administration of CB7 (2 mg/kg of CB7 in 10% DMSO, 10% Tween80, and 80% saline at 2 mg/mL) 5 minutes prior to radiotracer administration.

Mice. Six male mice C57BL/6J (Jackson Laboratories) were used for PET imaging. Anesthesia was achieved with isoflurane in medical oxygen carrier (3% for induction, 1% for maintenance, periodically adjusted to maintain a breathing rate of 30–70/minutes). For intravenous administration, a needle with an extension line was placed in a lateral tail vein.

PET/computed tomography image acquisition. After injection of a radiotracer bolus, a 60-minute dynamic PET scan was acquired. The PET scans were performed on a GammaMedica Triumph PET/CT/SPECT scanner, corrected for attenuation with a μ -map derived from the corresponding computed tomography (CT) image, which was acquired immediately before the PET scan. The dynamic PET data were binned into 38 time frames (8×15 seconds, 8×1 minutes, 10×2 minutes, 6×5) and reconstructed individually via an iterative maximum likelihood expectation maximization algorithm in 16 iterations.

Image analysis. The PET images were coregistered to the CT image acquired from the same animal using AMIDE. Regions of interest were placed according to the CT image. Whole brain time–activity curves were generated by AMIDE, and peripheral data were averaged from 30 to 60 minutes after extraction and both plotted with GraphPad Prism 7. Whole-body mouse images were visualized using AMIRA (Thermo Scientific).

Acknowledgments

We thank Judit Sore for radioisotope production and Michael S. Placzek for assistance with imaging experiments.

Declaration of Conflicting Interests

The author(s) declared no potential conflicts of interest with respect to the research, authorship, and/or publication of this article.

Funding

The author(s) disclosed receipt of the following financial support for the research, authorship, and/or publication of this article: We acknowledge the US Department of Energy (DE-SC0008430), the Phyllis and Jerome Lyle Rappaport MGH Research Scholar Award, the National Center for Research Resources (P41RR14075), and the Athinoula A. Martinos Center for Biomedical Imaging for resource support, including through NIH shared instrumentation (grants S10RR029495, 1S10RR017208-01A1, 1S10RR015728-01, S10RR022976, S10RR019933, and S10RR023401). L.I. thanks the NSF (CHE-1404911) for financial support.

References

- Mach JP, Buchegger F, Forni M, et al. Use of radiolabelled monoclonal anti-CEA antibodies for the detection of human carcinomas by external photoscanning and tomoscintigraphy. *Immunol Today*. 1981;2(12):239–249.
- Goldenberg DM, DeLand F, Kim E, et al. Use of radiolabeled antibodies to carcinoembryonic antigen for the detection and localization of diverse cancers by external photoscanning. *N Engl J Med*. 1978;298(25):1384–1386.
- Order SE. The history and progress of serologic immunotherapy and radiodiagnosis. *Radiology*. 1976;118(1):219–223.
- Kraeber-Bodéré F, Rousseau C, Bodet-Milin C, et al. A pretargeting system for tumor PET imaging and radioimmunotherapy. *Front Pharmacol*; 6. Epub ahead of print 2015. doi:10.3389/fphar.2015.00054.
- Schoffelen R, Boerman OC, Goldenberg DM, et al. Development of an imaging-guided CEA-pretargeted radionuclide treatment of advanced colorectal cancer: first clinical results. *Br J Cancer*. 2013;109(4):934–942.
- Stickney DR, Anderson LD, Slater JB, et al. Bifunctional antibody: a binary radiopharmaceutical delivery system for imaging colorectal carcinoma. *Cancer Res*. 1991;51(24):6650–6655.
- Marquez BV, Lapi SE. Pretargeted immuno-PET: overcoming limitations of space and time. *J Nucl Med*. 2016;57(3):332–334.
- Houghton JL, Zeglis BM, Abdel-Atti D, Sawada R, Scholz WW, Lewis J. Pretargeted immuno-PET of pancreatic cancer: overcoming circulating antigen and internalized antibody to reduce radiation doses. *J Nucl Med*. 2016;57(3):453–459.
- Van De Watering FCJ, Rijpkema M, Perk L, Brinkmann U, Oyen WJ, Boerman OC. Zirconium-89 labeled antibodies: a new tool for molecular imaging in cancer patients. *Biomed Res Int*; 2014. Epub ahead of print 2014. doi:10.1155/2014/203601.
- Frampas E, Rousseau C, Bodet-Milin C, et al. Improvement of radioimmunotherapy using pretargeting. *Front Oncol*; 3. Epub ahead of print 2013. doi:10.3389/fonc.2013.00159.
- Sharkey RM, Chang CH, Rossi EA, McBride WJ, Goldenberg DM. Pretargeting: taking an alternate route for localizing radionuclides. *Tumor Biol*. 2012;33(3):591–600.
- Liu G, Mang'era K, Liu N, Gupta S, Rusckowski M, Hnatowich DJ. Tumor pretargeting in mice using (99m)Tc-labeled morpholino, a DNA analog. *J Nucl Med*. 2002;43(3):384–391.
- Mardirossian G, Lei K, Rusckowski M, et al. In vivo hybridization of technetium-99m-labeled peptide nucleic acid (PNA). *J Nucl Med*. 1997;38(6):907–913.
- Goldenberg DM, Rossi EA, Sharkey RM, McBride WJ, Chang CH. Multifunctional antibodies by the dock-and-lock method for improved cancer imaging and therapy by pretargeting. *J Nucl Med*. 2007;49(1):158–163.
- Altai M, Perols A, Tsourma M, et al. Feasibility of affibody-based bioorthogonal chemistry-mediated radionuclide pretargeting. *J Nucl Med*. 2016;57(3):431–436.
- Patra M, Zarschler K, Pietzsch H-J, Stephan H, Gasser G. New insights into the pretargeting approach to image and treat tumours. *Chem Soc Rev*. 2016;45(23):6415–6431.
- Knight JC, Cornelissen B. Bioorthogonal chemistry: implications for pretargeted nuclear (PET/SPECT) imaging and therapy. *Am J Nucl Med Mol Imaging*. 2014;4(2):96–113.
- Karacay H, Sharkey RM, McBride WJ, et al. Pretargeting for cancer radioimmunotherapy with bispecific antibodies: role of the

- bispecific antibody's valency for the tumor target antigen. *Bioconjug Chem.* 2002;13(5):1054–1070.
19. Goldenberg DM, Chatal J-F, Barbet J, Boerman O, Sharkey RM. Cancer imaging and therapy with bispecific antibody pretargeting. *Update Cancer Ther.* 2007;2(1):19–31.
 20. Hnatowich DJ, Virzi F, Rusckowski M. Investigations of avidin and biotin for imaging applications. *J Nucl Med.* 1987;28(8):1294–1302.
 21. Goldenberg DM, Chang CH, Sharkey RM, et al. Radioimmunotherapy: is avidin-biotin pretargeting the preferred choice among pretargeting methods? *Eur J Nucl Med Mol Imaging.* 2003;30(5):777–780.
 22. Forster GJ, Santos EB, Smith-Jones PM, Zanzonico P, Larson SM. Pretargeted radioimmunotherapy with a single-chain antibody/streptavidin construct and radiolabeled DOTA-biotin: strategies for reduction of the renal dose. *J Nucl Med.* 2006;47(1):140–149.
 23. van de Watering FCJ, Rijpkema M, Robillard M, Oyen WJ, Boerman OC. Pretargeted imaging and radioimmunotherapy of cancer using antibodies and bioorthogonal chemistry. *Front Med.* 2014;1:1–11.
 24. He J, Liu GZ, Gupta S, Zhang Y, Rusckowski M, Hnatowich DJ. Amplification targeting: a modified pretargeting approach with potential for signal amplification – proof of a concept. *J Nucl Med.* 2004;45(6):1087–1095.
 25. Rossin R, Lappchen T, van den Bosch SM, Laforest R, Robillard MS. Diels-Alder reaction for tumor pretargeting: in vivo chemistry can boost tumor radiation dose compared with directly labeled antibody. *J Nucl Med.* 2013;54(11):1989–1995.
 26. Hou C, Huang Z, Fang Y, Liu J. Construction of protein assemblies by host–guest interactions with cucurbiturils. *Org Biomol Chem.* 2017;15(20):4272–4281.
 27. Assaf KI, Nau WM. Cucurbiturils: from synthesis to high-affinity binding and catalysis. *Chem Soc Rev.* 2015;44(2):394–418.
 28. Ma D, Hettiarachchi G, Nguyen D, et al. Acyclic cucurbit[n]uril molecular containers enhance the solubility and bioactivity of poorly soluble pharmaceuticals. *Nat Chem.* 2012;4(6):503–510.
 29. Walker S, Oun R, McInnes FJ, Wheate NJ. The potential of cucurbit[n]urils in drug delivery. *Isr J Chem.* 2011;51(5-6):616–624.
 30. Moghaddam S, Yang C, Rekharsky M, et al. New ultrahigh affinity host-guest complexes of cucurbit[7]uril with bicyclo[2.2.2]octane and adamantane guests: thermodynamic analysis and evaluation of M2 affinity calculations. *J Am Chem Soc.* 2011;133(10):3570–3581.
 31. Chen H, Hou S, Ma H, Li X, Tan Y. Controlled gelation kinetics of cucurbit[7]uril-adamantane cross-linked supramolecular hydrogels with competing guest molecules. *Sci Rep*; 6. Epub ahead of print 2016. doi:10.1038/srep20722.
 32. Rossin R, Verkerk PR, Van Den Bosch SM, et al. In vivo chemistry for pretargeted tumor imaging in live mice. *Angew Chemie – Int Ed.* 2010;49(19):3375–3378.
 33. Yu Y, Li J, Zhang M, Cao L, Isaacs L. Hydrophobic monofunctionalized cucurbit[7]uril undergoes self-inclusion complexation and forms vesicle-type assemblies. *Chem Commun.* 2015;51(18):3762–3765.
 34. Štimac A, Šekutor M, Mlinarić-Majerski K, Frkanec L, Frkanec R. Adamantane in drug delivery systems and surface recognition. *Molecules*; 22. Epub ahead of print 2017. doi:10.3390/molecules22020297.
 35. Liu W, Huang X, Placzek M, et al. Site-selective ¹⁸F fluorination of unactivated C–H bonds mediated by a manganese porphyrin. *Chem Sci.* Epub ahead of print 2017. doi:10.1039/C7SC04545J.
 36. Huang X, Liu W, Hooker JM, Groves JT. Targeted fluorination with the fluoride ion by manganese-catalyzed decarboxylation. *Angew Chemie – Int Ed.* 2015;54(48):5241–5245.
 37. Wang C, Schroeder FA, Wey HY, et al. In vivo imaging of histone deacetylases (HDACs) in the central nervous system and major peripheral organs. *J Med Chem.* 2014;57(19):7999–8009.